Ad Hoc Networks 87 (2019) 146–156

Contents lists available at ScienceDirect

Ad Hoc Networks

journal homepage: www.elsevier.com/locate/adhoc

Geometric aspects of probabilistic broadcasting in ad hoc networks

Felipe Forero R.[a], Néstor M. Peña T.[a], Nelson L.S. da Fonseca[b,*]

[a] Electronics and Telecommunication Systems Group (GEST), Department of Electrical and Electronic Engineering, Universidad de los Andes, Cra. 1E No. 19A 40, Bogota 111711, Colombia

[b] Institute of Computing, Campinas State University, Av. Albert Einstein, 1251, Cidade Universitaria, Campinas, SP 13083-852, Brazil

ARTICLE INFO

Article history:
Received 8 April 2018
Accepted 30 November 2018
Available online 15 December 2018

MSC:
00-01
99-00

Keywords:
Probabilistic broadcast
Signal to interference
Node layout
Network geometry

ABSTRACT

This paper studies pure probabilistic broadcast in ad hoc networks under a variety of topological scenarios, offering a comparison of the performance of broadcast in lattice-like geometric node layouts (e.g. nodes arranged in triangular, square and hexagonal grids) with that in randomly placed nodes. Results suggest that the geometry of the position of nodes has an impact on the success of probabilistic broadcast techniques. Specifically, networks with randomly-placed nodes exhibit a near-ideal (collision-free) behavior, whereas the grid layouts are extremely sensitive to the impact of collisions and interference. To account for the unreliable behavior of broadcast under certain node-distribution geometries, this paper provides an analysis of Signal to Interference ratio for ad hoc networks.

1. Introduction

In wireless ad hoc networks, nodes have no knowledge about the network topology, which makes broadcasting a fundamental building block for topology discovery and other network functions. Existing standards for broadcasting in ad hoc networks rely on a broadcast technique called *Flooding* [1]. In *Flooding*, every node receiving a broadcast message for the first time simply retransmits a copy of the message; under reliable (or almost ideal) channel conditions, this guarantees that messages reach all nodes in the network (i.e. 100% *reachability*). However, it has been shown that, in realistic wireless channels (i.e. when interference, delays, transmission errors, noise and radio-wave propagation features are considered), *Flooding* may not perform well [2], allowing the transmission of many redundant messages, leading to energy waste and channel contention.

To discuss the feasibility of using other protocols instead of *Flooding*, various broadcasting techniques, based on deterministic and probabilistic principles, have been assessed [3]. Despite producing minimum redundancy of broadcast messages, deterministic techniques depend on collecting topological information (i.e. transmitting additional control messages) and increase the complexity of the broadcast process, which can be more expensive than *Flooding* in dynamic topologies [4] and large-scale networks [5]. Recent studies [6] have illustrated the advantages of forwarding broadcast messages at random to reduce redundancy and produce low overhead. This is known as *probabilistic broadcasting* and consists of assigning probability threshold values (i.e. the so called *forwarding probability*) to individual nodes to decide whether a copy of the message received should be forwarded or not.

Performance evaluations of the simplest probabilistic protocols, conducted in test-beds [7–10], confirm the advantages of probabilistic broadcasting. However, the results suggest limitations in the average reachability of transmitted messages, as well as the dependence of the reachability of transmitted messages on the position of the broadcasting source; these issues are not anticipated by existing models of probabilistic broadcasting.

Most probabilistic broadcasting models assume an *ideal* wireless channel [11–14], and only a few models consider a *given* value for the probability of unsuccessful message reception [10,15]; little attention has yet been given to the incorporation of the *causes* of unsuccessful reception (as in [16]) in these probabilistic broadcasting models.

Moreover, in most studies (both in test-beds or based on simulation) [6], the limitation in reachability of transmitted messages and the efficiency of probabilistic broadcasting protocols under realistic conditions are associated with the calculation of the forwarding probability value (i.e. the strategy used to avoid the redundancy of *Flooding*). Performance limitations are rarely associ-

* Corresponding author.
E-mail addresses: f.rodriguez22@uniandes.edu.co (F. Forero R.), npena@uniandes.edu.co (N. M. Peña T.), nfonseca@ic.unicamp.br (N. L.S. da Fonseca).

https://doi.org/10.1016/j.adhoc.2018.11.014
1570-8705/

ated with other factors, such as the position of nodes in the network.

The present study was designed to help understand the causes of the limitations in the reachability of transmitted messages, especially the impact of the position of nodes, while taking into consideration realistic assumptions about channel conditions.

In line with this, Signal to Interference Ratio (S/I), which has been successfully applied to the design of Cellular Networks [17], has been employed in this paper to help analyze the impact of *the geometry of node distribution* on the protocol performance. Similar to Ramos et al. [18] for improving network lifetime in large-scale sensor networks, the geometrical features of network layouts are identified here as a factor that significantly affects the success of probabilistic broadcasting protocols in static networks with a few thousand nodes. Simulation results indicate that networks with randomly-placed nodes exhibit a *near-optimum* (near collision-free) behavior, while grid layouts are extremely sensitive to the impact of node interference.

The contribution of this paper is twofold:

- The incorporation of realistic assumptions (i.e. S/I model) in the analysis of the causes of the limitations in reachability of transmitted messages in probabilistic broadcasting schemes.
- An analysis of the impact of the geometry of network layouts on the reachability of probabilistic broadcasting protocols, as well as the greater strength of the influence of the node geometry in comparison to the impact of the position of the source node.

The present analysis is important for an understanding of applications involving hundreds of static nodes in which the geometry of network layout is a key factor in network performance. Results are relevant for grid-like geometries [19–22], for random geometries [23–25], and, in general, for terrestrial static sensor networks and environmental applications [26,27].

The rest of this paper is organized as follows. Section 2 summarizes previous evaluations of existing probabilistic broadcasting techniques. Section 3 introduces a *Signal to Interference* analysis that illustrates the significant impact of node placement distributions on the reachability of ad hoc broadcasting. Section 4 presents two sets of simulation results, and finally, Section 5 concludes the paper presenting a summary of the most relevant findings of the study.

2. Related work

The purpose of the present paper is to discuss some previously unexplored causes for failure of models proposed for probabilistic broadcasting protocols which assume the existence of an ideal channel. This section focuses on a set of studies that have already assessed the performance of probabilistic ad hoc broadcasting schemes and have observed existing models lacking precision under realistic settings using both simulation and experimentation in test-beds.

One of the first studies addressing the success of probabilistic broadcasting [28] identified that the network size and node degree impact on the avoidance of the *phase transition phenomenon* (i.e. a sudden transition from reaching less than 20% of the nodes to over 90% of the nodes with a small change in the forwarding probability). However, the collision-prone conditions were only implemented for randomly placed nodes. Grid scenarios were employed primarily to show the absence of the phase transition. Despite the inclusion of a moderate number of nodes in the random-placement scenarios, the authors clearly showed that, under realistic MAC-layer conditions, forwarding probability values should be carefully chosen so as to obtain the most from the pure-probabilistic broadcasting principle. Specifically, it was shown that, in more realistic, collision-prone environments, there is a maximum broadcasting success ratio when the probability of forwarding a message is as low as $p = 0.1$. As the probability increases, a larger number of collisions occur and, as a consequence, very few nodes can receive broadcast messages. The experiments designed to assess the effects of packet collisions in [28] were conducted using various simultaneous broadcasting sources, which makes it difficult to identify whether or not most of the collisions occurred as a consequence of self-interference of a message with its own copies or as a consequence of random collision of different messages.

More recent studies [10] introduced a retry-based scheme to improve reachability of the broadcast messages. By using both test-beds and simulation, the authors corroborated that interference and collisions must be included in probabilistic broadcasting models to allow for accurate predictions. The authors even proposed mapping between a more elaborate percolation model [29] and their retry-based scheme that could be used in future work to capture the behavior of the experiments adequately. Again, the conditions for inducing a high-interference environment were oriented by the use of many simultaneous broadcast sources. The interference caused by this large number of simultaneous sources was only tackled experimentally by adjusting the frequency of retries and little attention was devoted to the possibility of a broadcast message interfering with its own copies. Since the diameter of the network allowed good reachability with just a few hops, the number of nodes causing interference with the same copy of a broadcast message decreased very rapidly with the distance (in hops) from the broadcasting source.

The same authors of Blywis et al. [10] have also reported empirical results suggesting that special attention should be given to the effects of channel interference on the expected behavior of probabilistic broadcasting [9], especially when multiple broadcasting sources transmit simultaneously. Evidence from the test-bed experiments indicated that probabilistic broadcasting techniques do not avoid the collision of broadcast messages and excessive overhead. This observation was supported by the fact that certain reachability limits could not be surpassed during the evaluation in the test-bed. These findings are consistent with more recent studies [30], in which the performance of a completely different family of probabilistic broadcasting schemes (based on dissimilarity metrics and Euclidian distances) also evinced the reachability limits associated with the same test-bed.

What is common to all of the studies described here is that the limited reachability and efficiency of probabilistic broadcasting protocols under realistic conditions are associated to the way the calculation of the forwarding probability is carried out (i.e. the strategy used to avoid the redundancy of *Flooding*); and performance limitations are rarely associated with the geometrical properties of node placement in the network. Since little attention has been devoted to addressing the impact of the positions of nodes and the incorporation of realistic channel conditions in models, the following sections discuss the advantages of integrating the expected geometrical properties of network-wide node placement distributions into the assessment of probabilistic broadcasting techniques.

3. Impact of geometrical node distribution on probabilistic broadcast

The analysis in this section shows that the geometrical distribution of nodes is crucial for the success of the delivery of messages in ad hoc networks with static nodes employing a probabilistic broadcasting protocol. It also shows the difference in broadcasting conditions existing in grid layouts and those in a random layout. The assumption of nodes being static makes possible the evaluation of the impact of the geometry of nodes on broadcast-

ing, while excluding potential effects due to node mobility. Moreover, the present analysis can be considered as a first step towards the understanding of the impact of node geometry resulting from mobility on broadcasting, since the random layout used in this paper captures the asymptotic behavior of some mobility models (an example can be found in [31]; the interested reader can also refer to Santi [32] for details on mobility models that converge to asymptotic node spatial distributions).

The same principles in [17] for the analysis of co-channel interference in Cellular Telephone Systems are employed for the study of variation in the Signal to Interference Ratio (S/I) as a function of the position of nodes with respect to the broadcasting source. The calculations of S/I serve to evaluate *the impact of self-interference of a broadcast message with its own copies in a single broadcasting wave, which is independent of collisions caused by high-rate traffic patterns*. Specifically, the values of S/I in two scenarios are calculated and compared, the first scenario corresponding to a regular node layout of degree 4 (i.e. square grid), and the second to a layout where nodes are placed at random.

Fig. 1 illustrates a broadcasting source node located to the left of a square grid where the transmission range of the nodes (r) can cover four neighbors (i.e. a regular geometric graph of degree four). Diagonal dashed lines show groups of nodes associated with the same hop distance from the broadcasting source (i.e. the 3 nodes at a one-hop distance from the source are Tier 1, and the 5 nodes at a two-hop distance are Tier 2). The figure also shows three double arrows explicitly indicating the Euclidian distance of one node in Tier 2 (the receiving node) with respect to the three nodes in Tier 1. This situation corresponds to a worst-case scenario in which all the nodes in the previous tier (i.e. Tier 1 of the figure) transmit at exactly the same time, causing maximum interference. In any situation, the Collision Avoidance procedure in the medium access protocol (CSMA/CA in Layer 2) reduces such interference. Indeed, the inclusion of such a worst-condition assumption leads to a lower-bound model of the impact of network geometry on broadcasting without needing to consider a detailed time-dependent analysis.

In the traditional analysis of collision events, only the two nearest nodes (nodes at distances d_1 and d_s) would be considered to determine the probability of successful message delivery, but the analysis carried out here considers the calculation of S/I at the receiving node, including the interference of all nodes located in the previous tier. This makes possible the inclusion of the impact of node distribution in the analysis.

Without loss of generality (as in Chapter 3 of Rappaport [17]), the S/I calculation assumes a two-ray pathloss model, in which the power of the signal received at a distance d from the transmitter can be estimated using the transmitted power P_t together with the gain and height of both the transmitting (G_t, h_t) and the receiving antennas (G_r, h_t) as follows:

$$P_r = P_t G_t G_r \frac{{h_t}^2 {h_r}^2}{d^4} \tag{1}$$

Consequently, for the receiving node in the second tier of Fig. 1, the value of S/I corresponds to:

$$\frac{S}{I} = \frac{P_t G_t G_r {h_t}^2 {h_r}^2 \dfrac{1}{{d_s}^4}}{P_t G_t G_r {h_t}^2 {h_r}^2 \left(\dfrac{1}{{d_1}^4} + \dfrac{1}{{d_2}^4} \right)} \tag{2}$$

where d_s is the distance between the expected transmitter from the previous tier and the receiving node, and d_1 and d_2 are the distances from the receiver to the other two transmitters from the previous tier (i.e. Tier 1). Assuming homogeneous characteristics of all nodes in the network (i.e. similar antenna heights, antenna gains and transmission power), the previous expresion reduces to:

$$\frac{S}{I} = \frac{\dfrac{1}{{d_s}^4}}{\left(\dfrac{1}{{d_1}^4} + \dfrac{1}{{d_2}^4} \right)} \tag{3}$$

By considering again Fig. 1, and the forwarding probability p in the analysis, Eq. (3) becomes:

$$\frac{S}{I} = \frac{\dfrac{1}{{d_s}^4}}{\left(I_{\{X_1 < p\}} \dfrac{1}{{d_1}^4} + I_{\{X_2 < p\}} \dfrac{1}{{d_2}^4} \right)} \tag{4}$$

where $I_{\{X_i < p\}}$ is the *indicator function*, and X_i is a random value drawn at the i-th node (i.e. $X \sim U([0, 1])$), such that $I = 1$ when $X_i < p$, otherwise $I = 0$. This includes, in Eq. (3), the Bernoulli variables that indicate whether or not nodes in the previous tier forward a broadcast message. Notice that the numerator has no *indicator function* because the intention is to calculate the average signal quality (S/I) only when broadcast messages are *received*, i.e. the calculation of *probabilistic interference* given that nodes receive messages from their expected previous-tier transmitter. The value of p, thus, dictates the reduction in interference as p decreases.

Finally, for an arbitrary receiver with n interferers (i.e. n nodes associated with the previous tier, excluding the expected transmitter), the calculation of *probabilistic* S/I corresponds to:

$$\frac{S}{I} = \frac{\dfrac{1}{{d_s}^4}}{\sum_{i=1}^{n} I_{\{X_i < p\}} \dfrac{1}{{d_i}^4}} \tag{5}$$

where d_s is the distance between the receiver and the expected transmitter whereas d_i is the distance between the receiver and the i-th interferer.

Indeed, Eq. (5) is a ratio of distances, for a single interferer $S/I = (d_s/d_1)^{-4}$. Therefore, what matters is the positions of the nodes relative to each other, and not the absolute distances (in meters). This highlights even more the fact that the geometry of nodes is a key issue in the S/I analysis.

Eq. (5) is used in the remainder of this section to calculate the S/I values for all nodes in the network. Notice that this calculation does not depend on the network layout (i.e. it is not restricted to the example in Fig. 1) and can be used to estimate the values of probabilistic S/I in any network as long as tiers can be established with respect to a broadcasting source. Besides that, other models of propagation different from the two-ray pathloss model would result in a similar equation. For example, for a more general propagation model such as the *log-distance path loss model with log normal shadowing* the only change in Eq. (5) would be the power of the Euclidian distances (known as the path-loss exponent), which would not be 4. Moreover, measurement studies [17] have reported that for urban environments (path-loss exponent between 3 and 5) as well as for indoor environments with obstacles (path-loss exponent between 4 and 6) the value 4 for the path-loss exponent can be used. A good example can be found in [33], using a path-loss exponent value of 4.2. Thus, results obtained using Eq. (5) are still general enough for the use of a more elaborate propagation model.

Suppose now that the square grid topology in Fig. 1 is part of a larger square-grid network (i.e. regular layout of degree 4). Fig. 2 illustrates a *larger-scale* view of the way tiers are created as a function of the position of the source. This 10-row, 13-column square grid illustrates how tiers take an angular shape, resembling two plane wavefronts that propagate away from the source (up to tiers

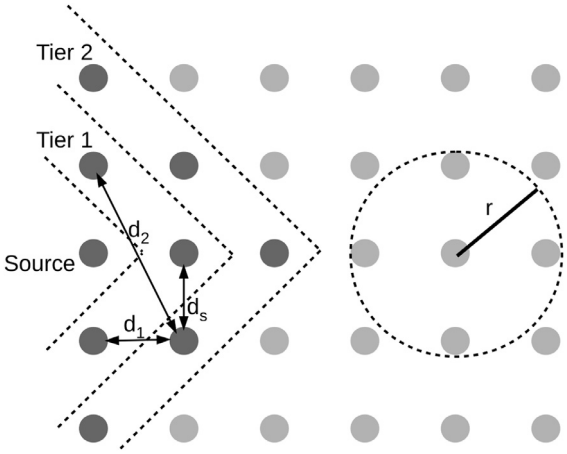

Fig. 1. *S*/*I* for a receiving node in the second tier, where interference comes from two of the three nodes in the first tier.

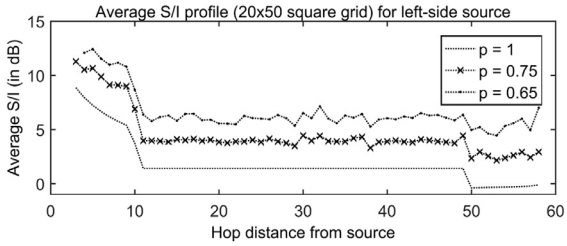

Fig. 3. *S*/*I* profile for nodes in the 20×50 grid of degree 4 as a function of the tier (i.e. hop distance to the broadcasting source). Three curves corresponding to three values of probability. Notice that lower probability leads to less interference, that is, better average *S*/*I*.

16 and 17 for nodes in the right-hand corners of the rectangular region). If this pattern is maintained for a 20×50 square grid, the farthest node would be seen in Tier 60. Fig. 3 illustrates the calculation of the probabilistic *S*/*I* values averaged for the 60 tiers of such a 20×50 grid with a source positioned in row 10 column 1. The *x*-axis indicates the tier, i.e. the hop-distance from the broadcasting source. The values of probabilistic *S*/*I* were calculated 100 times and the average per node was calculated. Finally, each point in Fig. 3 shows the average of probabilistic *S*/*I* values per tier. For example, for Tier 2, one value of *S*/*I* is obtained from 5 nodes; for Tier 3, the result is obtained from 7 nodes, and so on. The main idea here is to observe how the average value of *S*/*I* varies as the broadcast message propagates away from the source. Fig. 3, thus, represents the variation in the quality of the received wireless signal as the distance, in hops, to the source node increases, that is, as the message propagates from left to right throughout the 20×50 grid. The values of the first two tiers were not included in the figure because the nodes in Tiers 1 and 2 produced very few interferers and several values of *S*/*I* were infinity.

Indeed, the *S*/*I* calculation gives the average quality of the signal for a worst-case broadcasting scenario in which transmitters are totally synchronized, leading to a maximum number of closest interferers (i.e. all interferers from the previous tier). Unlike some deterministic broadcasting algorithms [34], synchronized nodes are not essential for the operation of the protocol, but make a worst-case assumption. For any other scenario, in which heterogeneous delays in nodes imply transmitters desynchronization, the Collision Avoidance procedure of nodes reduces interference, and as a consequence, the *S*/*I* values are expected to be higher than those in Fig. 3. Thus, the curves in the figures in this section represent lower bounds for the *S*/*I* values.

Higher values of *S*/*I* imply greater chances of successfully propagating broadcast messages over additional tiers. Moreover, nodes near the farthest corners of the region would have a low rate of successfully received messages, since these nodes lack neighbors, rather than because of the low values of *S*/*I*. Such reacha-

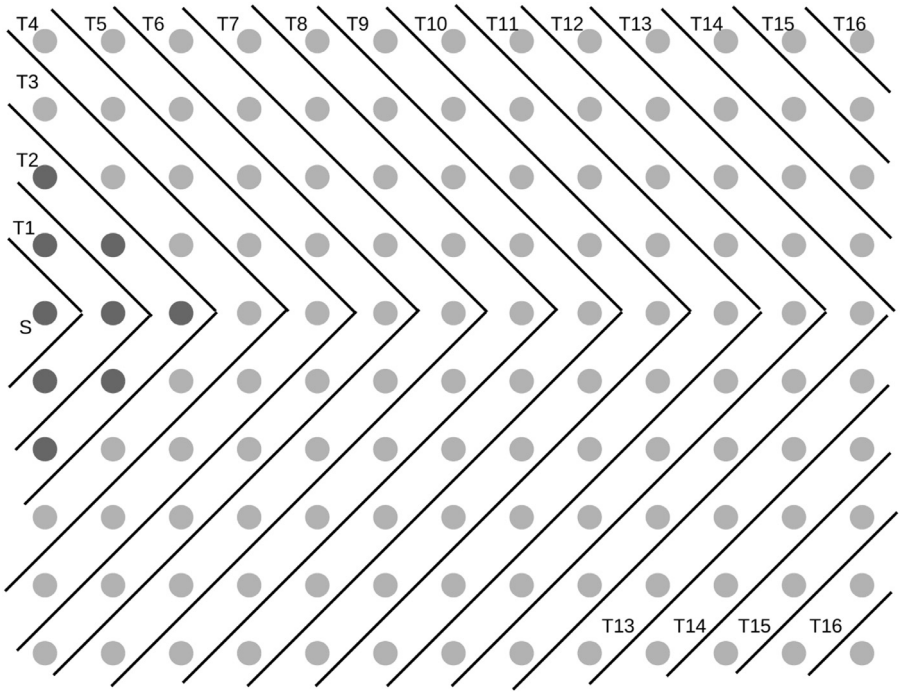

Fig. 2. A zoom-out representation of Fig. 1 for 10 rows and 13 columns of a square grid with the source node on the left (row 5 column 1 of the grid). Solid lines indicate the shape of the expected tiers (angle-shaped tiers) propagating the message from left to right. The minimum number of hops to reach the node in the top-right corner is 16 (i.e. Tier 16).

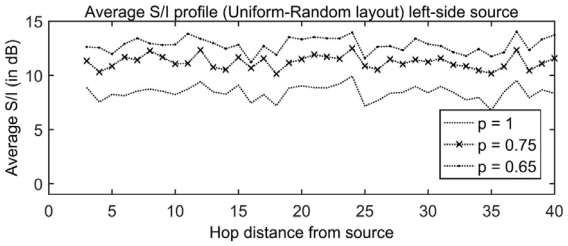

Fig. 4. *S*/*I* profile for random node placement as a function of the hop distance from the source. Lower probability yields higher *S*/*I* values. This profile is more stable than that for the grid.

bility in the last tiers is independent of the geometry, as shown in Section 4.

The role of the geometry of nodes can be better emphasized when comparing the *S*/*I* values in Fig. 3 with those presented in the measurement-based studies in [35]. For example, in the first 10 tiers, an *S*/*I* value around 10 dB would result in nearly 100% of successfully received messages at low rates of 1 Mbp, which is a standard broadcast rate [1], while for nodes located at more than 10 tiers from the source, with *S*/*I* values between 2 dB and 6 dB, the percentage of successful transmissions would not exceed 50%. Moreover, regardless of the forwarding probability, the curves in Fig. 3 clearly reveal three network segments, namely Tiers ≤ 10 (receiving the highest *S*/*I* values), $11 \leq$ Tiers ≤ 49 and $50 \leq$ Tiers. These three segments are the points at which the propagation of broadcast messages reaches the edges of the rectangular area. This may indicate that the relation between the geometry of node position (grid of degree 4) and the shape of the area where the nodes reside (a rectangle) also has an impact on the average quality of the channel to receive broadcast messages. This impact is as significant as the impact of the forwarding probability value, since the difference between the curves for $p = 1$ to $p = 0.65$ is similar to that between *S*/*I* values in tiers $1 - 10$ and tiers $10 - 50$ for all the three curves.

It is worth mentioning that the values of p chosen for the *S*/*I* curves in Fig. 3 are well supported by the literature on probabilistic broadcasting [6]. In general, values between 0.6 and 0.75 are of great interest since they lead to minimum levels of redundancy (i.e. maximum Saved Rebroadcast, SRB in the literature) while maintaining the reachability of transmitted messages at over 90%. In the majority of investigations on probabilistic broadcast the optimal value of p is around 0.7, except for studies in which the average node density is over 10 nodes within the transmission range, for which the optimal values of p are far lower than 0.7.

Now the calculation of probabilistic *S*/*I* in Eq. (5) is applied to another rectangular region, also containing 1000 nodes, but with these nodes located *at random* according to a uniform distribution (see Fig. 5). The transmission range of the nodes (r) was set at 250 m and the dimensions of the rectangle at $7500\,\text{m} \times 3000\,\text{m}$. As in [36], this setting leads to a high probability of having a connected network [37,38]. This means that, if there is a smaller value of r, fewer nodes, or a larger region, a considerable proportion of random layouts would result in disconnected networks, which impacts the performance of broadcast. Additionally, this setting has the same ratio of height to width for the sides of the rectangular area (i.e. 2: 5 ratio as the 20×50 square grid). To make a fair comparison with the results of the grid, 100 different random layouts were derived. For each random layout, tiers were established with respect to the nodes located closest to the point (0,1500) (left center nodes) so that left-to-right propagation of broadcast messages was maintained. Results for random placement are shown in Fig. 4.

Results in Figs. 3 and 4 indicate that the random setting exhibits higher values of *S*/*I* and far more stable conditions for broadcast messages to propagate from the source node towards the end of the network. For example, in the square grid, with the lowest interference conditions ($p = 0.65$), the *S*/*I* remained below 8 dB from tier 10 onwards. Meanwhile, with the random layout and the highest interference ($p = 1$), *S*/*I* was always above 7 dB. Based on the results, it is important to point out that interference has a stronger impact on the grid, where nodes have fewer neighbors, than on the random layouts, in which nodes have an average of eight neighbors. This is equivalent to saying that nodes with fewer neighbors suffered more interference because they are distributed in a grid, whereas nodes with a higher number of neighbors (on average) experience less interference due to the randomness of their relative positions.

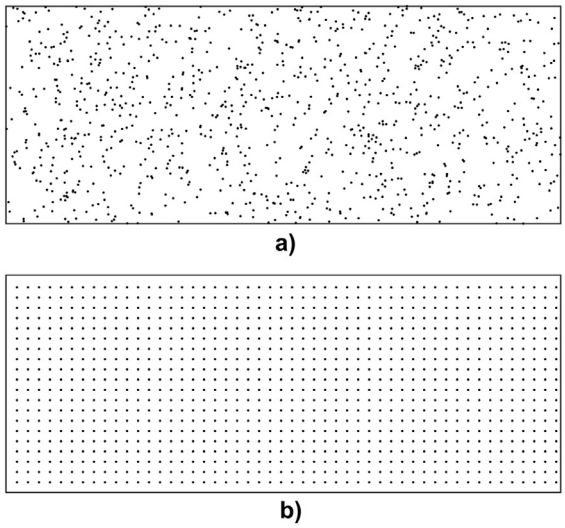

Fig. 5. Large-scale view of the positions of 1000 nodes for (a) the random scenario and (b) the 20×50 square grid in two rectangular regions with equivalent height-width ratio.

The analysis in this section yields three important observations. First, there are aspects specific to the geometry of ad hoc networks (namely, the distribution of node placement) that may significantly affect the performance of probabilistic broadcasting techniques. Second, it seems that random settings offer more stable conditions for the propagation of broadcast messages. Finally, by integrating the Euclidian distance in the analysis, the *S*/*I* calculation can be used to predict the expected success of ad hoc probabilistic broadcasting messages as a function of the network-wide node distribution.

4. Simulation experiments

4.1. Random and regular placement of nodes

The previous section showed that, for realistic wireless channels, ad hoc networks with random layouts facilitate the propagation of broadcast messages more than do grid layouts. To further verify this conclusion, the present section shows results about the performance of probabilistic broadcast derived via simulation. The simulator used was Qualnet v7.3 [39]. Table 1 displays the values of the simulation parameters. The two network scenarios correspond to the square grid and the network with random placement of nodes described in the previous section. Nodes in the first four tiers forward broadcast messages with a probability of $p = 1$. This difference in scenarios was adopted for comparison with the results in [36], which used a technique called *GOSSIP1(p,k)*. The work in [36] was taken as benchmark because the authors offered a good comparison of probabilistic broadcasting performance em-

Table 1
Simulation settings.

Parameter	Value
Number of nodes	1000
Area of Uniform Random	7500 m × 3000 m
Area of 20 × 50 grid	12500 m × 5000 m
Transmission Range	250 m approximately
Path-loss model	Two-ray
Mobility	none
Mac Layer	802.11
Technique	*GOSSIP1(p,4)*
Source Position	left-center
Runs	120 replications

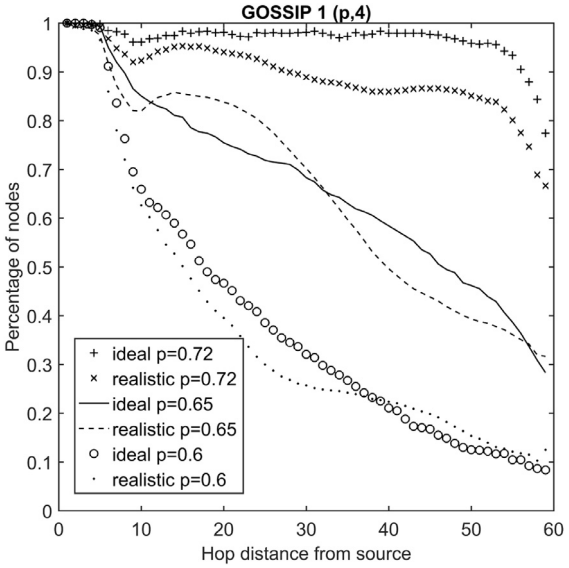

Fig. 6. Comparison of probabilistic broadcasting success as a function of node distance to the broadcasting source, for three values of p. Collision-less, ideal conditions vs. realistic conditions for the 20×50 grid.

ploying both grids and random node layouts. The parameters of *GOSSIP1* are p for the forwarding probability, and k for the number of tiers where nodes use $p = 1$ (i.e. the simulations were run with *GOSSIP1(p,4)*). The results in [36] were derived with the assumption of an ideal MAC layer, so the following comparison illustrates the impact of realistic conditions on the performance of probabilistic broadcast, which reinforces the observations in Section 3. The values of p in the present study are the same as those used in [36], since values for p around 0.7 provide maximum reachability with the minimum number of message copies, especially for the scenarios considered in this section. Values higher than 0.75 would lead to a higher probability of collisions and waste of energy and bandwidth, whereas values lower than 0.6 would result in a considerable reduction in reachability (reachability near 20%) [7,28].

Figs. 6 and 7 show the impact on probabilistic broadcasting performance when employing realistic channels instead of ideal ones. These figures measure the percentage of nodes reached by broadcast messages as a function of the node distance, in hops, from the broadcast source (i.e. percentage of nodes of the same tier). When realistic conditions affect the performance, the most noticeable difference is for the case of the square grid with forwarding probability $p = 0.72$ (Fig. 6), in which reachability decreases by more than 15% after 30 hops. As the probability decreases in the grid scenario, the gap between results for the *ideal* and *realistic* channels also decreases, since an *emptier* channel resembles an ideal channel.

The realistic curves for $p = 0.72$ and $p = 0.65$ in the square grid (Fig. 6) show a sudden drop after Tier 10, as predicted by the decrease in the average S/I values shown in Fig. 3. Such a drop can be associated with the interplay between the rectangular shape of the area containing the nodes and the position of the source node; indeed, for the left-hand centered position of the source in the 20×50 grid, the propagation of the message meets the first border of the network at hop 10.

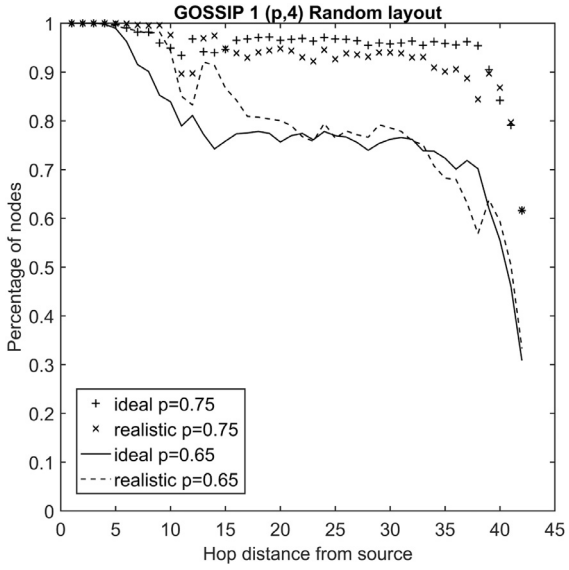

Fig. 7. Comparison of broadcast reachability under ideal conditions vs. more realistic conditions for Uniform Random Node Distribution with $p = 0.75$ and $p = 0.65$.

In [36], a slightly higher probability value ($0.75 > 0.72$) for the random scenario was employed to achieve a reachability similar to that of the grid scenario. When realistic conditions are considered, however, the curves for $p = 0.65$ show that the random scenario does not require a higher probability value in order to match (or even outperform) the reachability of grid scenarios, as confirmed in Section 4.2.

What is common for all the probability values evaluated in Fig. 6 is that reachability values in the *ideal* curves show a smoother decrease than their *realistic* counterparts. In fact, the realistic curves oscillate more, reaching more nodes than do the ideal curves in some of the tiers (as is the case of $p = 0.65$ between hop-distance 12 and 30). Oscillating curves may arise when many nodes of one tier successfully receive a broadcast message, so that transmission to the next tier has to tolerate maximum interference. However, when only a few nodes receive the message, their transmissions to the next tier will produce low values of interference, increasing the chances of successful broadcast propagation in subsequent tiers.

Fig. 7 shows that the percentage of nodes receiving the message in different tiers (hop-distance) is almost the same for both the *ideal* and *realistic* scenarios. In fact, for $p = 0.65$, the curves after hop 22 are almost identical, whereas before hop 22, the realistic curve reached a higher fraction of nodes. Such a trend is consistent with the S/I analysis in Section 3, shown in Fig. 4. The broadcasting propagation offered by the randomly-placed node layouts is stable, even for the worst-case scenario of the interference analysis.

These results reinforce the need for analyzing the impact of the geometry of ad hoc networks on the performance of probabilistic broadcasting, as described in Section 3, especially when observing that:

- Random network-wide node distributions promote the success of probabilistic broadcasting transmissions in realistic scenarios more than do grid layouts.

- The geometry of node distribution should be considered in the performance of ad hoc probabilistic broadcasting.

In order to draw more general conclusions, the following section explores the consistency of these findings. By changing the position of the source node, different patterns of broadcast transmission should be seen. The following section also shows the impact of using other geometries such as a triangular grid, a larger square grid, and hexagonal grid, as well as variations in random distributions (e.g. Uniform, Normal, Poisson).

4.2. Other grid geometries and node distributions

This section provides a broader view of the relation between probabilistic broadcasting and node placement by exploring more general scenarios that involve various different grid layouts, as well as random node distributions. The following simulation results also extend the discussion about the impact of the position of the broadcasting source on broadcasting reachability, motivated by previous work [7,8] in a test bed, which showed that results are strongly dependent on the position of the source node.

The simulation parameters are those in Table 1. However, in this section, the number of nodes and the shape of the area vary. The following results were obtained with 2500 nodes within a square region (e.g. a 7000×7000 square region for the random settings). For the random settings employing the Normal and the Poisson distributions, the number of nodes is *on average* 2500 since the number of nodes is also a random variable. Every single replication of the simulation was run using a different set of random numbers for both the forwarding decisions and the random node positions. Therefore, the results capture the average behavior of node distributions and avoid the potential bias of using a single geometrical realization for all replications. Having such a variety of scenarios (120 for each random distribution) using a test bed would be prohibitive, but it is feasible using simulations, as has been done here. Moreover, the different random positions of nodes in each replication can be seen as snapshots of a mobile network; since the density functions of the random variables that determine the positions of nodes at different times converge to a unique density function in the long run (cf. [31]). A mobility model with such a property is said to be *stationary* [32].

As in the previous sections, the figures show the reachability profile of probabilistic broadcast, namely the fraction of nodes that sucessfully receive broadcast messages as a function of the node distance, in hops, from the source (i.e. the tier). Moreover, the figures are organized to illustrate the impact of changing the position of the source node, which in turn changes the conditions for the propagation of messages.

Figs. 9 to 11 show the behavior of probabilistic broadcasting in 50×50 grids in which nodes (except the nodes forming the sides of the grid) have three, four, or six neighbors. Hereinafter the prefix *Tri* will corespond to the regular grid of degree six (i.e. triangular grid), the prefix *Sq* to the grid of degree four (i.e. square grid), and the prefix *Hex* to the grid of degree three (i.e. hexagonal grid or honeycomb grid). Fig. 9 focuses on all scenarios with broadcasting sources located in one of the four corners of the square region. Figs. 10 and 11 show the curves for scenarios with broadcasting sources on one side and at the center of the grids, respectively. In the figures, the curve length depends on the grid. The Tri-grid curves are always the shortest. In these figures, the longest curves always correspond to the grid of degree three (i.e. Hex-Grid), which has 123 tiers for the corner source, more than 110 tiers for sources on the side of the grid, and 63 tiers when the source lies at the center of the grid. Fig. 8 shows how the topology of an Hex-grid leads to fewer nodes per tier than does its Tri-grid counterpart. As a consequence, the Tri-grid needs less tiers to cover the same number of nodes. This figure can be compared to Fig. 2 to further illustrate how the number of tiers (x-axes in the figures) was obtained for each simulation scenario.

For geometrically regular node placement, the Tri-grid is consistently the most favorable setting for the success of probabilistic broadcasting. For example, with the source located in the corner, for $p = 0.6$, the broadcast messages reached slightly fewer than 80% of the nodes from tier 15 to 55, while for $p = 0.65$ and $p = 0.72$, messages reached over 90% of the nodes. This occured because the triangular grid has more *collision-free* nodes receiving messages in every tier than the other grids. For example, when the source is at the center of the grid, in the worst case scenario in which all nodes from the same tier transmit at the same time, the triangular grid still guarantees that at least six nodes can propagate the message in all directions with no risk of collision. For a source node at the center, the square grid offers only four collision-free receivers per tier and the hexagonal grid only three collision-free nodes per tier. Similar geometrical limitations can be shown for sources on the side and in the corner of grids. However, for the hexagonal grid, collisions due to time-correlated propagation of broadcast messages occur only every two tiers. This lack of redundancy means that, for every collision-free tier, the use of probabilistic broadcasting simply reduces reachability, similar to the propagation of broadcast for nodes lying in a straight line. This explains the negative-exponential shape of the curves (curves of the Hex-grid), almost resembling the graph of a geometric sequence for the value of p (recall that $0 < p < 1$).

Moving the source to one side, and then to the center, always improves reachability. In the first tiers, a sudden decrease in reachability occurs, even before the fourth tier. This is somewhat unexpected since we know that broadcast packets are forwarded with $p = 1$ for the first four tiers. This early drop in the curves is more accentuated when the source is in the corner (Fig. 9). As the message propagates over the tiers, either the same reachability is kept until the end of the network or reachability increases, suggesting that, under *realistic* collision-prone conditions, the unreliable delivery of the MAC layer occurs mostly in the first tiers, due to the highly correlated times when forwarding messages from the same source. After the first collisions occur and the message propagates farther from the source, forwarding times gradually lose correlation and facilitate the operation of the CSMA/CA mechanism, which explains the shape of the curves.

The number of collision-free nodes per tier is extremely important in providing robustness. Namely, for the triangular grid, the curves for $p = 0.72$ show almost the same performance as the curves for $p = 0.65$, which represents a 10% reduction in the number of messages forwarded, but the reachability is still the same. Moreover, the curves for the same probabilities differ significantly in other grids.

The impact of having a finite network is noticeable in Fig. 9. Specifically, for sources in the corner, there is a consistent *tweak* at around tier 50 for all curves, which is the tier where the sides of the network end. This *tweak* is even more noticeable with the broadcasting source on the side (Fig. 10), where a marked change can be observed in all curves at around tier 25 (the tier at which the broadcast propagation wave encounters the firts borders of the square region). In these two figures, there is always a segment of the curves, which corresponds to the transmission encountering the border, when the broadcasting process simply recovers, reaching a larger percentage of the nodes than in previous tiers. Conversely, when the source is at the center of the grid (Fig. 11), the curves always decrease, although some slight changes can also be observed at tier 25, where the number of nodes per tier begins to drop. These patterns can be explained by the way the number of nodes changes on a tier as the message propagates. For example, the square grid with *the source on the side* has 3 nodes in Tier 1, 5

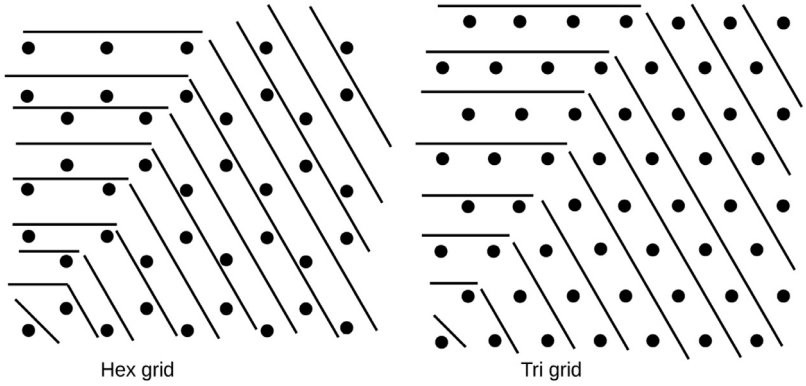

Fig. 8. Comparison of the shape of tiers for the Hex-grid and Tri-grid for sources in the bottom left corner. The Tri-grid covers more nodes in each tier. Consequently, for grids of the same dimensions the Tri-grid results in less tiers than both the Hex-grid and the Sq-grid.

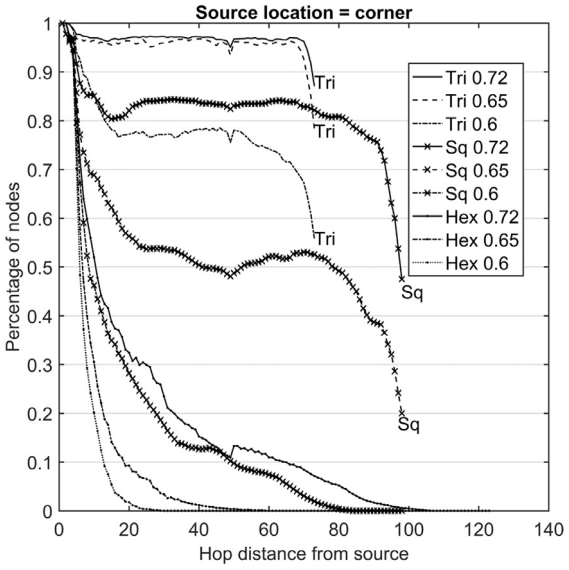

Fig. 9. Reachability when the source node is located in one corner of the grid. The *x*-axis shows the hop distance from the source while the *y*-axis indicates the average percentage of nodes that received the message at particular distances (i.e. on average, the percentage of the tier that received broadcast messages).

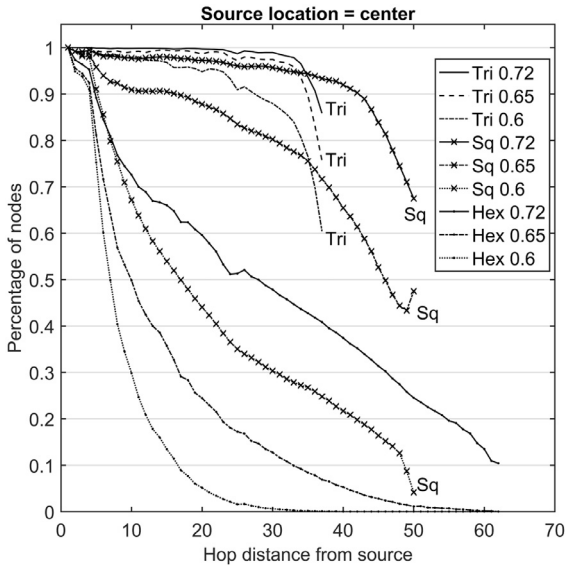

Fig. 11. Reachability when the source node is located at the center of the grid (geometrically regular node placement scenarios only).

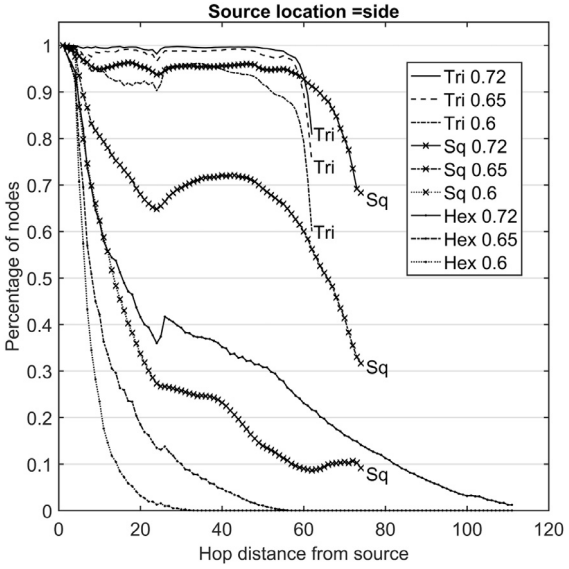

Fig. 10. Reachability when the source node is located on one side of the grid (geometrically regular node placement scenarios only).

nodes in Tier 2, 7 nodes in Tier 3, and so on, until tier 25. As the size of the tier increases, the number of nodes in the border of the square region represents a smaller percentage of the tier. At hop 25, the size of the tier and the proportion of its border nodes stabilizes (remaining 51 nodes with two nodes on the border of the region) until hop 49, where the size of the tier decreases continuously to the edge of the network. It can be affirmed that a stable behavior of the probabilistic broadcasting phenomenon can only be seen for 25 tiers (from tier 25 until tier 49). After this, the shape of the curves will be closely related to the proportion of border nodes per tier.

For the three random network scenarios (Figs. 12–14), the overall performance is more stable than that of grids, as suggested by the analysis in Section 3. Even with the lowest probability, when the broadcasting source is in the corner (Fig. 12 with probability $p = 0.6$), the fraction of nodes reached by broadcast messages was always over 80%. As the source moved to the side (Fig. 13), and then to the center of networks (Fig. 14), reachability always improved. It is important to mention that all random scenarios were set using the theoretical *Critical Transmitting Range for Connectivity*, which is defined as the minimum value of r (i.e. the transmission range) such that the resulting communication graph is connected. It is important to recall that a graph is connected if and

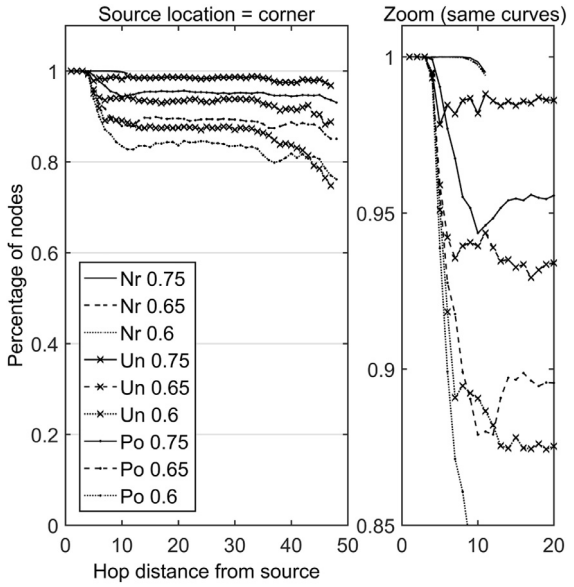

Fig. 12. Reachability for Geometric random networks as a function of hop distance from the source (source node located in one corner of the network). These Figures include a plot zoom on the right so that the curves for the Normal distribution can be observed in the same scale as the other six curves.

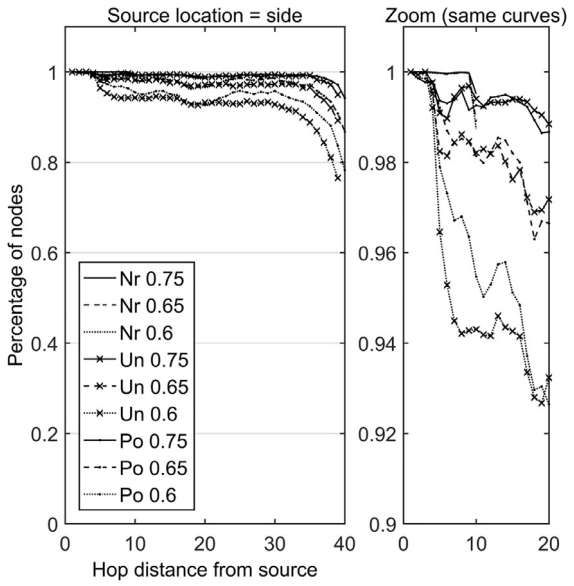

Fig. 13. Reachability for Geometric random networks as a function of hop distance from the source (source node located on one side of the network). Notice the zooming on the right for visualization of the curves associated with the Normal distribution.

only if there exists at least one path connecting any two nodes in the graph. For the particular case of the random Normal distribution, a detailed view of the first values of the graph was necessary (see the right side of Figs. 12–14), since these networks had a very small diameter. This situation results from maintaining connectivity when employing the Normal distribution, since for this distribution the *Critical Transmitting Range for Connectivity* [40] is greater than those for the Uniform and Poisson [38] distributions. Despite the reduced number of observable tiers for the Normally distributed node layouts, reachability was even greater than in the scenarios with Uniform and Poisson distributions.

What is common in these figures is the impact of the position of the source node on broadcast reachability. Regardless of the situation (whether grids or random placement), it is clear that when the source is in the corner, the lowest reachability is obtained in all scenarios. In fact, results for sources located in a corner can be taken as a lower bound for performance, which is important for design purposes (cf. test-bed results in [7,8]). Indeed, results confirm that any other position for the source node, other than the corner of the region, would result in greater reachability. Meanwhile, when the source is on the side, the wave of broadcast seems to pass through segments of recovery where reachability is greater than for previous tiers. The figures also show that centered sources always result in the greatest reachability, despite showing monotone decreasing reachability values (i.e. no segments of recovery or stability).

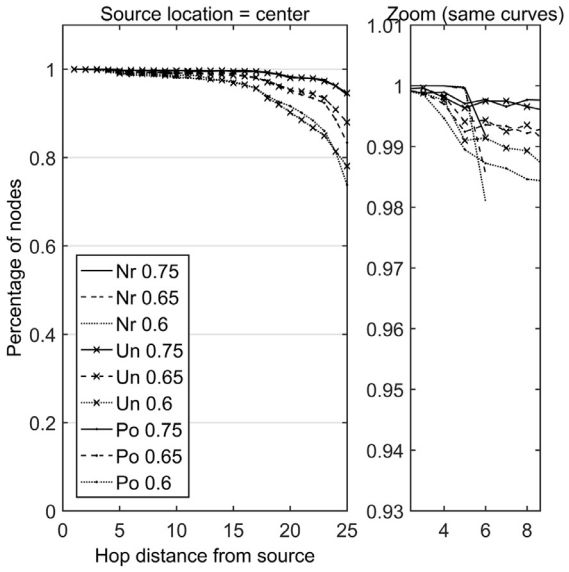

Fig. 14. Reachability for Geometric random networks as a function of hop distance from the source (source node located at the center of the network).

Finally, the random layouts reduce the highly-correlated forwarding times that degrade the performance of probabilistic broadcasting in geometrically regular layouts, facilitating the operation of the CSMA/CA mechanism to avoid collisions, especially in the first tiers of a single-message broadcast propagation event. This property provides random layouts with *robustness* against the effects of collisions when applying probabilistic broadcasting in ad hoc networks.

5. Conclusions

The present paper has highlighted the impact of node placement on the success of probabilistic broadcasting in large-scale static ad hoc networks when realistic wireless channels are considered. The calculation of *S*/*I* levels revealed that random placement of nodes facilitates propagation of broadcast messages, while nodes arranged in grids face reachability limitations. *S*/*I* analysis (borrowed from the co-channel interference analysis of cellular networks) has made possible the integration of the Euclidian geometry of node position with the benefits of probabilistic broadcasting, and this should be considered for future development of ad hoc probabilistic broadcasting protocols.

The observations obtained in the analysis have been further confirmed by running a comprehensive set of complementary simulations that included more and larger grids with different geometries, as well as more geometrically random scenarios. The evidence clearly indicates that grid layouts render ad hoc networks extremely sensitive to the impact of realistic conditions.

Conversely, when nodes are placed at random, the behavior of probabilistic broadcasting appears to reflect more ideal conditions.

The results also reveal that the use of tiers to characterize the propagation of broadcast messages facilitates the analysis of broadcast reachability profiles, providing detailed information about the broadcasting process e.g. the interplay between the shape of the area surrounding the network and the position of the source node. Furthermore, realistic reachability profiles show an oscillating pattern as a function of the distance in hops from the broadcast source, with tiers receiving a large percentage of broadcast messages being followed by tiers with low reachability, and vice versa. This suggests that, after a series of collision events, there will be a series of successful broadcast events as a consequence of the previous reduction in potential broadcast interferers. Under ideal conditions, these collisions would not occur and the oscilating pattern is not observed.

The benefits of studying non-conventional causes of pure-probabilistic broadcast failure (e.g. geometrical features rather than node density or broadcasting rates) under non-ideal wireless conditions are two-fold. First, the simplicity of pure-probabilistic broadcasting leads to faster broadcasting waves, which is convenient for overcoming the effects of node mobility and should have a positive impact on higher-level network functions, such as Admission Control when applied to different routing protocols [41]. Second, for scenarios where grids are relevant [19–22], simple, yet effective, countermeasures can be adopted to avoid poor performance of their ad hoc broadcast protocols.

Future work should include the study of latency and mobility under various geometrical conditions. Simulations of large-scale networks like the one in [19] should be analyzed in order to assess the feasibility of real probabilistic-broadcasting implementations. The analysis in this paper, including the ideas in [28], about changes in the behavior of broadcast reachability depending on network size and node degree, should be conducted in order to evaluate the impact of geometry on small networks. Also, probabilistic broadcasting and the impact of geometry can be integrated in the performance evaluation of MAC layer protocols in a multi-hop context [42].

Acknowledgements

This work was supported by Departamento Administrativo de Ciencia, Tecnologḍa e Innovacin (Departamento Administrativo de Ciencia, Tecnología e Innovación - CTel - República de Colombia) under call for grants 617 (2013) for National Doctoral Degrees, Conselho Nacional de Desenvolvimento Cientḍfico e Tecnolgico and grant # 15/24494-8, São Paulo Research Foundation (FundaA̋o de Amparo Pesquisa do Estado de So Paulo).

References

[1] L.M.S.C. of the IEEE Computer Society, IEEE Standard 802.11–2012, Technical Report, LAN/MAN Standards Committee of the IEEE Computer Society, IEEE 3 Park Avenue New York, NY 10016-5997 USA, 2012.

[2] S.-Y. Ni, Y.-C. Tseng, Y.-S. Chen, J.-P. Sheu, The broadcast storm problem in a mobile ad hoc network, in: Proceedings of the 5th Annual ACM/IEEE International Conference on Mobile Computing and Networking, in: MobiCom '99, ACM, New York, NY, USA, 1999, pp. 151–162, doi:10.1145/313451.313525.

[3] B. Williams, T. Camp, Comparison of broadcasting techniques for mobile ad hoc networks, in: Proceedings of the 3rd ACM International Symposium on Mobile Ad Hoc Networking &Amp; Computing, in: MobiHoc '02, ACM, New York, NY, USA, 2002, pp. 194–205, doi:10.1145/513800.513825.

[4] F. Dai, J. Wu, Performance analysis of broadcast protocols in ad hoc networks based on self-pruning, in: 2004 IEEE Wireless Communications and Networking Conference (IEEE Cat. No.04TH8733), 2, 2004, pp. 802–807Vol.2, doi:10.1109/WCNC.2004.1311289.

[5] S. Basagni, M. Mastrogiovanni, C. Petrioli, A performance comparison of protocols for clustering and backbone formation in large scale ad hoc networks, in: 2004 IEEE International Conference on Mobile Ad-hoc and Sensor Systems (IEEE Cat. No.04EX975), 2004, pp. 70–79, doi:10.1109/MAHSS.2004.1392076.

[6] D. Reina, S. Toral, P. Johnson, F. Barrero, A survey on probabilistic broadcast schemes for wireless ad hoc networks, Ad Hoc Netw. 25, Part A (2015) 263–292, doi:10.1016/j.adhoc.2014.10.001. http://www.sciencedirect.com/science/article/pii/S1570870514002169.

[7] B. Blywis, M. Günes, F. Juraschek, S. Hofmann, Gossip routing in wireless mesh networks, in: 21st Annual IEEE International Symposium on Personal, Indoor and Mobile Radio Communications, 2010, pp. 1572–1577, doi:10.1109/PIMRC.2010.5671949.

[8] B. Blywis, M. Güneş, S. Hofmann, F. Juraschek, A study of adaptive gossip routing in wireless mesh networks, in: Ad Hoc Networks - Second International Conference, ADHOCNETS 2010, Victoria, BC, Canada, August 18–20, 2010, Revised Selected Papers, 2010, pp. 98–113, doi:10.1007/978-3-642-17994-5_7.

[9] B. Blywis, M. Guenes, F. Juraschek, O. Hahm, Challenges and limits of flooding and gossip routing based route discovery schemes, in: Local Computer Networks (LCN), 2011 IEEE 36th Conference on, 2011, pp. 283–286, doi:10.1109/LCN.2011.6115304.

[10] B. Blywis, P. Reinecke, M. Günes, K. Wolter, Gossip routing, percolation, and restart in wireless multi-hop networks., in: WCNC, IEEE, 2012, pp. 3019–3023. http://dblp.uni-trier.de/db/conf/wcnc/wcnc2012.html#BlywisRGW12.

[11] B. Williams, D.P. Mehta, T. Camp, W. Navidi, Predictive models to rebroadcast in mobile ad hoc networks, IEEE Trans. Mob. Comput. 3 (3) (2004) 295–303, doi:10.1109/TMC.2004.25.

[12] H. Zhang, Z.-P. Jiang, Performance analysis of broadcasting schemes in mobile ad hoc networks, IEEE Commun. Lett. 8 (12) (2004) 718–720, doi:10.1109/LCOMM.2004.837658.

[13] H. Zhang, Z.-P. Jiang, Modeling and performance analysis of ad hoc broadcasting schemes, Perform. Eval. 63 (12) (2006) 1196–1215, doi:10.1016/j.peva.2005.12.002. http://www.sciencedirect.com/science/article/pii/S016653160500177X.

[14] I.S. Lysiuk, Z.J. Haas, Controlled gossiping in ad hoc networks, in: 2010 IEEE Wireless Communication and Networking Conference, 2010, pp. 1–6, doi:10.1109/WCNC.2010.5506346.

[15] V. Drabkin, R. Friedman, G. Kliot, M. Segal, On reliable dissemination in wireless ad hoc networks, IEEE Trans. Dependable Secure Comput. 8 (6) (2011) 866–882, doi:10.1109/TDSC.2010.54.

[16] K. Viswanath, K. Obraczka, Modeling the performance of flooding in wireless multi-hop ad hoc networks, Comput. Commun. 29 (8) (2006) 949–956. Performance Evaluation of Wireless Networks and Communications, doi: 10.1016/j.comcom.2005.06.015. http://www.sciencedirect.com/science/article/pii/S0140366405002173.

[17] T.S. Rappaport, Wireless Communications Principles and Practice (2nd Edition) Hardcover, 2 edition, Prentice Hall PTR, 2001. http://openlibrary.org/books/OL9286375M.

[18] H.S. Ramos, A. Boukerche, A.L. Oliveira, A.C. Frery, E.M. Oliveira, A.A. Loureiro, On the deployment of large-scale wireless sensor networks considering the energy hole problem, Comput. Netw. 110 (2016) 154–167, doi:10.1016/j.comnet.2016.09.013. http://www.sciencedirect.com/science/article/pii/S1389128616303036.

[19] S. Savazzi, L. Goratti, D. Fontanella, M. Nicoli, U. Spagnolini, Pervasive uwb sensor networks for oil exploration, in: Ultra-Wideband (ICUWB), 2011 IEEE International Conference on, 2011, pp. 225–229, doi:10.1109/ICUWB.2011.6058833.

[20] S. Savazzi, U. Spagnolin, Synchronous ultra-wide band wireless sensors networks for oil and gas exploration, in: Computers and Communications, 2009. ISCC 2009. IEEE Symposium on, 2009, pp. 907–912, doi:10.1109/ISCC.2009.5202244.

[21] F. Zhixin, Y. Yue, Condition health monitoring of offshore wind turbine based on wireless sensor network, in: 2012 10th International Power Energy Conference (IPEC), 2012, pp. 649–654, doi:10.1109/ASSCC.2012.6523345.

[22] C. Bajracharya, R. Grodi, D.B. Rawat, Performance analysis of wireless sensor networks for wind turbine monitoring systems, in: SoutheastCon 2015, 2015, pp. 1–4, doi:10.1109/SECON.2015.7133053.

[23] G. Simon, M. Maróti, A. Lédeczi, G. Balogh, B. Kusy, A. Nádas, G. Pap, J. Sallai, K. Frampton, Sensor network-based countersniper system, in: Proceedings of the 2Nd International Conference on Embedded Networked Sensor Systems, in: SenSys '04, ACM, New York, NY, USA, 2004, pp. 1–12, doi:10.1145/1031495.1031497.

[24] L. Krishnamurthy, R. Adler, P. Buonadonna, J. Chhabra, M. Flanigan, N. Kushalnagar, L. Nachman, M. Yarvis, Design and deployment of industrial sensor networks: Experiences from a semiconductor plant and the north sea, in: Proceedings of the 3rd International Conference on Embedded Networked Sensor Systems, in: SenSys '05, ACM, New York, NY, USA, 2005, pp. 64–75, doi:10.1145/1098918.1098926.

[25] K.-K. Yap, V. Srinivasan, M. Motani, Max: Human-centric search of the physical world, in: Proceedings of the 3rd International Conference on Embedded Networked Sensor Systems, in: SenSys '05, ACM, New York, NY, USA, 2005, pp. 166–179, doi:10.1145/1098918.1098937.

[26] J. Yick, B. Mukherjee, D. Ghosal, Wireless sensor network survey, Comput. Netw. 52 (12) (2008) 2292–2330, doi:10.1016/j.comnet.2008.04.002. http://www.sciencedirect.com/science/article/pii/S1389128608001254.

[27] I. Akyildiz, W. Su, Y. Sankarasubramaniam, E. Cayirci, Wireless sensor networks: a survey, Comput. Netw. 38 (4) (2002) 393–422, doi:10.1016/S1389-1286(01)00302-4. http://www.sciencedirect.com/science/article/pii/S1389128601003024.

[28] Y. Sasson, D. Cavin, A. Schiper, Probabilistic broadcast for flooding in wireless mobile ad hoc networks, in: Wireless Communications and Networking, 2003. WCNC 2003. 2003 IEEE, 2, 2003, pp. 1124–1130 vol.2, doi:10.1109/WCNC.2003.1200529.

[29] L. Nduwayo, R. Lindebaum, N. Chetty, Suppressed bond-site percolation, Comput. Phys. Commun. 180 (4) (2009) 503–508. Special issue based on the Conference on Computational Physics 2008CCP 2008. doi: 10.1016/j.cpc.2009.01.027. http://www.sciencedirect.com/science/article/pii/S1389128601003024.
[30] D. Reina, M. Günes, S. Toral, Real experimentation of probabilistic broadcasting algorithms based on dissimilarity metrics for multi-hop ad hoc networks, Ad Hoc Netw. 47 (2016) 1–15, doi:10.1016/j.adhoc.2016.04.002. http://www.sciencedirect.com/science/article/pii/S1570870516300981.
[31] M. Nitti, L. Atzori, Modeling of network connectivity in multi-homed hybrid ad hoc networks, in: L. Atzori, J. Delgado, D. Giusto (Eds.), Mobile Multimedia Communications, Springer Berlin Heidelberg, Berlin, Heidelberg, 2012, pp. 307–320.
[32] P. Santi, Mobility models for next generation wireless networks: ad hoc, vehicular and mesh networks, Wiley, 2012.
[33] G. Colistra, L. Atzori, Estimation of physical layer performance in WSNs exploiting the method of indirect observations, J. Sens. Actuator Netw. 1(3) (2012) 272–298, doi:10.3390/jsan1030272. https://www.researchgate.net/publication/278915920_Estimation_of_Physical_Layer_Performance_inWSNs_Exploiting_the_Method_of_Indirect_Observations.
[34] S. Basagni, D. Bruschi, I. Chlamtac, A mobility-transparent deterministic broadcast mechanism for ad hoc networks, IEEE/ACM Trans. Netw. 7 (6) (1999) 799–807, doi:10.1109/90.811446.
[35] A. Kashyap, S. Ganguly, S.R. Das, Measurement-based approaches for accurate simulation of 802.11-based wireless networks, in: Proceedings of the 11th International Symposium on Modeling, Analysis and Simulation of Wireless and Mobile Systems, in: MSWiM '08, ACM, New York, NY, USA, 2008, pp. 54–59, doi:10.1145/1454503.1454516.
[36] Z.J. Haas, J.Y. Halpern, L. Li, Gossip-based ad hoc routing, IEEE/ACM Trans. Netw. 14 (3) (2006) 479–491, doi:10.1109/TNET.2006.876186.
[37] M. Penrose, Random geometric graphs, Oxford studies in probability, Oxford University Press, 2003. https://books.google.co.uk/books?id=M38e7nPGSCsC
[38] P. Santi, Topology control in wireless ad hoc and sensor networks, Wiley, 2005. https://books.google.ie/books?id=XPxSAAAAMAAJ.
[39] Qualnet simulator http://web.scalable-networks.com/qualnet-network-simulator-software Last accessed: 2017-06-09.
[40] M.D. Penrose, Extremes for the minimal spanning tree on normally distributed points, Adv. Appl. Probab. 30 (1998) 628–639, doi:10.1017/S000186780000851X. http://journals.cambridge.org/article_S000186780000851X.
[41] M. Salamanca, N. Peña, N. da Fonseca, Impact of the routing protocol choice on the envelope-based admission control scheme for ad hoc networks, Ad Hoc Netw. 31 (2015) 20–33, doi:10.1016/j.adhoc.2015.03.008. http://www.sciencedirect.com/science/article/pii/S157087051500058X.
[42] J. Alonso-Zrate, C. Crespo, C. Skianis, L. Alonso, C. Verikoukis, Distributed point coordination function for ieee 802.11 wireless ad hoc networks, Ad Hoc Netw. 10 (3) (2012) 536–551, doi:10.1016/j.adhoc.2011.09.004. http://www.sciencedirect.com/science/article/pii/S1570870511001958.

Felipe Forero received his M.Sc. degree in Communication and Information Sciences from Universidad Distrital FJC, Bogotá, Colombia in 2012. Currently, he is member of the Electronics and Telecommunication Systems Group (GEST) at Universidad de los Andes, where he is Ph.D. candidate in Electrical Engineering. In 2014, he was awarded with a scholarship from COLCIENCIAS (Departamento Administrativo de Ciencia, Tecnología e Innovación - CTel - República de Colombia) to pursue a doctoral degree. His research interests are communication protocols for wireless networks and signal processing.

Nestor Misael Peña is Electrical Engineer, Mathematician and M.Sc. in electrical engineer from Universidad de Los Andes, Bogotá, Colombia. He received his D.E.A and Ph.D. degree in telecommunications and signal treatment from the University of Rennes 1 in 1994 and 1997, respectively. Currently, he is full professor in the Department of Electrical and Electronics Engineering at Universidad de los Andes. His research interests are modeling and evaluation of communication protocols in ad hoc and sensor networks, development of numerical methods in electromagnetism at very high frequencies, and electromagnetic compatibility.

Nelson Luis Saldanha da Fonseca received his Ph.D. degree from University of Southern California in 1994. Nelson is a Full Professor at the Institute of Computing, State University of Campinas. He received the 2001 Elsevier Computer Network Editor of the Year and the IEEE Communications Society (ComSoc) Joseph LoCicero Award for Exemplary Services in Publications. Nelson Fonseca is former EiC of the IEEE Communications Surveys and Tutorials. Currently, he serves as Associate Editor for Elsevier Computer Networks, Senior Editor for the IEEE Communications Magazine and for the IEEE Communications Surveys and Tutorials and Editor for the Journal of Internet Services and Applications, Peer-to-Peer Networking and Applications. Nelson Fonseca is VP Technical and Educational Activities for ComSoc and also served as ComSoc VP Publications.